Soft Matter

Accepted Manuscript

ROYAL SOCIETY OF CHEMISTRY

www.rsc.org/softmatter

Effect of local chain deformability on the temperature-induced morphological transitions of polystyrene-*b*-poly(*N*-isopropylacrylamide) micelles in aqueous solution

Xi-Xian Ke[1], Lian Wang[2], Jun-Ting Xu[1],* Bin-Yang Du[1], Ying-Feng Tu[3],

Zhi-Qiang Fan[1]

[1]MOE Key Laboratory of Macromolecular Synthesis and Functionalization, Department of Polymer Science & Engineering, Zhejiang University, Hangzhou 310027, China
[2]College of Material, Chemistry and Chemical Engineering, Hangzhou Normal University, Hangzhou 310036, China
[3]Department of Polymer Science and Engineering, College of Chemistry, Chemical Engineering and Materials Science, Soochow University, Suzhou, 215123, P. R. China.

Submitted to *Soft Matter*

(revised)

2014-05-09

*Correspondence author. E-mail: xujt@zju.edu.cn , Tel./Fax: +86-571-87952400

Abstract

The effect of temperature on the micellar morphology of two polystyrene-*b*-poly(*N*-isopropylacrylamide) (PS-*b*-PNIPAM) diblock copolymers in aqueous solution was investigated by dynamic light scattering (DLS) and transmission electron microscopy (TEM). At 25 ℃, mixture of vesicles and spheres are observed for the micelles of PS_{65}-*b*-$PNIPAM_{108}$, while PS_{65}-*b*-$PNIPAM_{360}$ exhibits mixed cylindrical and spherical micellar morphology. Upon raising temperature, the micellar morphology becomes spherical for PS_{65}-*b*-$PNIPAM_{108}$ at 60 ℃ and PS_{65}-*b*-$PNIPAM_{360}$ at 40 ℃. Such vesicle-to-sphere and cylinder-to-sphere transitions of micellar morphology are reversible when the micellar solutions are cooled back to 25 ℃. However, such temperature-induced morphological transitions of PS-*b*-PNIPAM micelles are opposed to the theoretical prediction. Qualitative analysis of the free energy shows that vesicular or cylindrical micelles tend to be formed at higher temperature, if only the overall volume change of the PNIPAM block is considered. The contradiction between the experimental results and theoretical prediction is interpreted in terms of the local deformability of the PNIPAM chains. At elevated temperature, the collapsed PNIPAM globules are less deformable and must occupy larger area at the micellar interface, though the overall volume is smaller than that at lower temperature. This will lead to larger repulsion between the PNIPAM globules and remarkable increase in the free energy of the corona, thus formation of vesicles or cylinders at higher temperature is prohibited.

1 Introduction

It is well known that amphiphilic block copolymers (BCPs) can self-assemble into micelles in a selective solvent above the critical micellization concentration (CMC).[1,2] The BCP micelles usually consist of a core formed by the insoluble block and a corona formed by the soluble block. When the thickness of the corona is much larger than that of the core, the micelle is star-like, whereas the micelle is crew-cut if the dimension of the corona is much smaller than that of the core.[3-5] BCP micelles may exhibit a variety of morphologies, including frequently reported sphere, cylinder and vesicle. The micellar morphology of BCPs is determined by the structure of BCPs (block length and block ratio) and external factors such as temperature, solvent quality and preparation method, etc.[6-13] Theoretical analysis shows that all above factors actually affect three items of Gibbs free energy: the free energy of the core (F_{core}) associated with the deformation of the core-forming block, the free energy of the corona (F_{corona}) reflecting the deformation of the corona-forming block and the free energy of the interface ($F_{interface}$) determined by the surface area of the core and the interaction between the solvent and the core.[14-18] For star-like micelles $F_{interface}$ and F_{corona} are dominant and $F_{interface}$ accounts for the majority of the overall free energy in crew-cut micelles.[18]

Under most conditions, the micellar morphology and the morphological transition of micelles can be qualitatively interpreted in terms of these three items of free energy. Calculation of $F_{interface}$ and F_{corona} is based on some overall parameters, such as the chain length, the excluded volume and the interface area occupied by per chain, etc.[17]

On the other hand, there exists a curvature for the interface of corona and core in the BCP micelles, which is larger for the spherical micelles but smaller for vesicles. The existence of interfacial curvature results in different local deformations of the corona-forming blocks, especially in the spherical star-like micelles. As shown in Scheme 1, the soluble block in a spherical star-like micelle can be viewed as close-packing of a series of concentric blobs with different sizes.[14,15] The contribution of each blob to the free energy of steric repulsion between the corona-forming blocks is ~ k_BT.[15] This leads to gradual decrease of the concentration of the corona-forming blocks as the distance to the interface increases,[14] which means that the conformation of the corona-forming blocks varies with the distance to the interface. As a result, the soluble block in the spherical star-like micelles must be flexible so that different local conformations can be adopted. We called the ability of polymer chains exhibiting different conformations at different positions inside the micelles as "local deformability". From this viewpoint, F_{corona} is related to not only the overall size of the soluble block but also its local deformability. For example, we assume that there are two types of polymer chains attached to the same core-forming blocks. One type of polymer chain is longer and flexible, which has a larger coil size and can form blobs of different sizes. The other is shorter and rigid. As compared with the former, the latter has a smaller coil size but is difficult to form blobs with variable diameters. What would the micellar morphologies be for these two BCPs? To our best knowledge, the local deformation of the soluble block is rarely considered in literature while discussing the micellar morphology of BCPs. In order to demonstrate the effect

of local deformability of the soluble block, herein we designed two polystyrene-*b*-poly(*N*-isopropylacrylamide) (PS-*b*-PNIPAM) BCPs and temperature-induced morphological transition of the micelles was investigated.

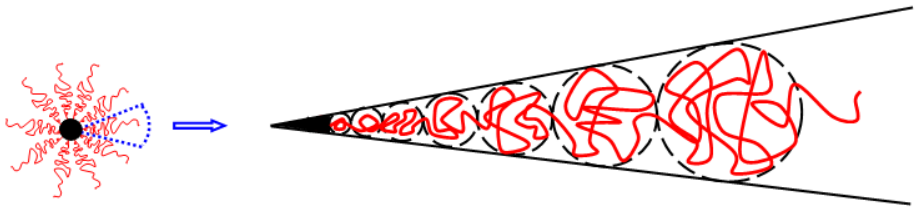

Scheme 1 Schematic illustration of different local deformations in the spherical star-like micelles.

PNIPAM is a type of thermally responsive polymer with a lower critical solution temperature (LCST) in water.[19,20] Below the LCST, hydrogen bonds can be formed between PNIPAM and water and PNIPAM is water-soluble. At the temperature above the LCST, the hydrogen bonds are destroyed, thus PNIPAM becomes hydrophobic and polymer chains collapse into globules.[21,22] The micellization and thermo-responsive behaviors of many PNIPAM-based BCPs have been extensively studied.[23-30] However, in most of the work only the change of the micelle size without alteration of the overall micellar morphology is reported.[31-34] Wu observed a transition of the micellar morphology from wormlike vesicles to spherical vesicles in dioxane/ethanol upon increasing temperature for a PS-*b*-PNIPAM formed by hydrogen bond at the end of both blocks.[35] Monteiro found that, the micellar morphology of a PS-*b*-PNIPAM at a high concentration in water, including sphere, rod and vesicle, could be regulated by sonication with the aids of temperature change

and/or addition of toluene.[36,37] Grubbs et al. observed that heating the micelles of poly(ethylene oxide)-*b*-poly(*N*-isopropylacrylamide)-*b*-poly(isoprene) triblock copolymer in the aqueous solution above the LCST of PNIPAM could induce a sphere-to-vesicle transition of the micellar morphology.[38] Such a transition is reversible upon cooling. Moughton et al. synthesized poly(*t*-butyl acrylate)-*b*-poly(*N*-isopropylacrylamide) and poly(methyl acrylate)-*b*-poly (*N*-isopropylacrylamide) BCPs bearing a hydrophilic head.[39,40] The sphere-to-vesicle transition of the micellar morphology in the aqueous solution was observed as well.

In the present work, temperature was utilized to alter the conformation of PNIPAM in the PS-*b*-PNIPAM BCPs. It is expected that the overall size of the PNIPAM block will change with temperature due to alteration of solvation degree. Moreover, the flexible random coil of PNIPAM below the LCST and the collapsed PNIPAM globule above the LCST may also exhibit different deformability. The effects of the overall coil size and local deformability on micellar morphology were discussed and compared with the theoretical prediction.

2 Experimental section

2.1 Materials

Styrene was first washed with an aqueous solution of sodium hydroxide (5 wt%) three times and with water until neutralization and then distilled under reduced pressure. *N*-Isopropylacrylamide (NIPAM, Aldrich) was purified by recrystallization from a mixture of benzene and *n*-hexane. 4,4′-Azobis(isobutyronitrile) (AIBN) (Fluka, 98%) were purified by recrystallization from ethanol. 1, 4-Dioxane was distilled from a

purple sodium ketyl solution. *S*-1-Dodecyl-*S*′-(α,α′-diemthyl-α″-acetic acid)trithiocarbonate (DDAT) was prepared according to the published procedure.[41] Tetrahydrofuran (THF) was refluxed with sodium flakes and distilled prior to use. Deionized water was distilled twice prior to use. Other reagents were used as received without further purification.

2.2 Preparation of PS-*b*-PNIPAM BCPs

PS-*b*-PNIPAM BCPs were prepared via sequential reversible addition fragmentation transfer (RAFT) polymerization, as described in our previous work.[42] Styrene was first polymerized in bulk with AIBN as the initiator and DDAT as the RAFT agent to yield PS-containing macro-RAFT agent, then polymerization of NIPAM was conducted in the presence of PS-containing macro-RAFT agent and AIBN in the second step after removal of un-polymerized styrene monomer. The detailed procedure for preparation of PS-*b*-PNIPAM BCPs and the characterization results are given in supplementary material (Figs. S1 and S2). The molecular characteristics of two PS-*b*-PNIPAM BCPs are listed in Table 1.

Table 1 The molecular characteristics of two PS-*b*-PNIPAM BCPs.

Sample	M_n [a]	PDI [b]	Chemical composition [a]	f_{PS} [c]
1	19330	1.16	PS_{65}-*b*-$PNIPAM_{108}$	36%
2	47800	1.26	PS_{65}-*b*-$PNIPAM_{360}$	15%

[a] Calculated from ^{1}H-NMR spectra. [b] PDI = M_w/M_n, determined by GPC. [c] Volume fraction of the PS block.

2.3 Preparation of the PS-*b*-PNIPAM micelles

The PS-*b*-PNIPAM BCP (1.5 mg) was first dissolved in 12.0 mL of THF to obtain a

homogeneous solution, then the solution was sealed in a cellulose dialysis tube with a cutoff molecular weight of 3500 g/mol and directly dialyzed against deionized water at 25 ℃ for 3 days to remove THF. The THF solvent was completely removed by exchanging with fresh water five times. After dialysis, the micellar solution was transferred to a clean volumetric flask and then a certain volume of deionized water was used to wash the dialysis bags and added to the flask to make the final solution volume of 25.0 mL. The resulting block copolymer solutions with such a low concentration (0.06 mg/mL) were used for both DLS and TEM analysis so that the results obtained by these two methods can be compared.

2.4 Instruments

Dynamic light scattering (DLS) measurements were performed on a Brookhaven Instrument BI-200SM with a laser wavelength of 636 nm at 25 ℃ at a scattering angle of 90 °. The data were analyzed with the software supplied by Brookhaven. The DLS measurements were also carried out at different scattering angles. The scattering angles θ were set from 45 to 135 ° at an interval of 15 °. At each angle, the data acquisition time was set to be 5 min. For measurements at different temperatures, the samples were kept at the required temperatures for at least 15 min before the data collection. For each sample, the heating or cooling experiments were repeated twice. The deviation of two measurements at each temperature was within 3 nm, showing good reproducibility of the experiments. The data presented are the average values.

Transmission electron microscopy (TEM) observations were carried out on a JEOL JEM-1230 electron microscope at an acceleration voltage of 80 kV. TEM

samples were prepared by dropping 4 μL of the micellar solution onto a carbon-coated copper grid. Excess fluid was then absorbed with a piece of filter paper. Subsequently, the samples on the grid were immediately frozen with liquid nitrogen and freeze-dried under the vacuum at -20 ℃ to avoid the reassembly and aggregation of the micelles during the drying process. To characterize the micellar morphology above the LCST, the micellar solutions kept at high temperatures (60 °C for PS_{65}-*b*-$PNIPAM_{108}$ and 40 °C for PS_{65}-*b*-$PNIPAM_{360}$) were used for sample preparation. The prepared samples were directly used for TEM observation without further staining.

3 Results and discussion

3.1 Thermo-responsive behavior of the PS-*b*-PNIPAM micelles

The change of the micellar size with temperature was first investigated. The micellar solutions were heated from room temperature to 60 °C and then cooled back to room temperature again. Fig. 1 shows the apparent hydrodynamic diameter (D_h) measured by DLS determined at various temperatures during the heating and cooling cycle. It is observed that D_h decreases drastically in a wide temperature range for the micelles of both PS-*b*-PNIPAM BCPs. A two-stepwise decrease in D_h is observed for the PS_{65}-*b*-$PNIPAM_{108}$ micelles. D_h first decreases rapidly before 35 ℃, which is near the LCST of PNIPAM, and there is also a sharp decrease in D_h between 55-60 ℃. As for the PS_{65}-*b*-$PNIPAM_{360}$ micelles, besides the quick decrease of D_h around 35 ℃, D_h is stable between 35-40 ℃ and then gradually decreases above 40 ℃. A two-stepwise decrease in the diameter was also reported for PNIPAM grafted on gold and silica

nanoparticles,[43,44] which was attributed to the different local segment concentrations in the inner region and outer region of the PNIPAM brushes. The inner region has a higher segment concentration and exhibits a lower LCST, while it is reverse for the outer region. As a result, the two-stepwise decrease in D_h supports our hypothesis that the local chain conformations of PNIPAM near and far from the interface of the micellar corona and core are different. We also notice that the change of the micellar size with temperature is completely reversible. When being cooled from 60 ℃ back to room temperature, the micelles basically recover to the original size. However, hysteresis is observed for the micellar size upon heating and cooling the micellar solutions. Such a phenomenon is also frequently observed for PNIPAM microgels and brushes.[45] The different intra- and inter-chain interactions in the collapsed and hydrated PNIPAM may lead to different thermal response rates in the heating and cooling processes. The scattering light intensity of the PS-*b*-PNIPAM micellar solutions also varies with temperature (Fig. S3 in supplementary material). For both PS-*b*-PNIPAM BCPs, there is a sharp change in the scattering light intensity around the LCST of PNIPAM. The change of the scattering light intensity with temperature is also reversible.

It is observed that, even the PS-*b*-PNIPAM micelles are heated to 60 ℃, at which the PNIPAM blocks are collapsed and become hydrophobic, the micelles are still stable at such a low concentration and can be well dispersed in the aqueous solution for a long time, as reported in literature.[46-48] Fig. 2 shows the values of D_h at different times for PS_{65}-*b*-$PNIPAM_{108}$ at 60 ℃ and PS_{65}-*b*-$PNIPAM_{360}$ at 40 ℃, respectively.

One can see that the micellar size is invariant with time for both BCPs, at least in the time scale studied. This enables us to study the micellar morphology above the LCST using other methods, such as TEM. Moreover, we notice that there is a larger difference between the micellar sizes at room temperature (below the LCST) and at the temperature above the LCST, especially for the PS_{65}-*b*-$PNIPAM_{360}$ micelles. This indicates that the micellar morphology may be altered when the micellar solutions are heated above the LCST.

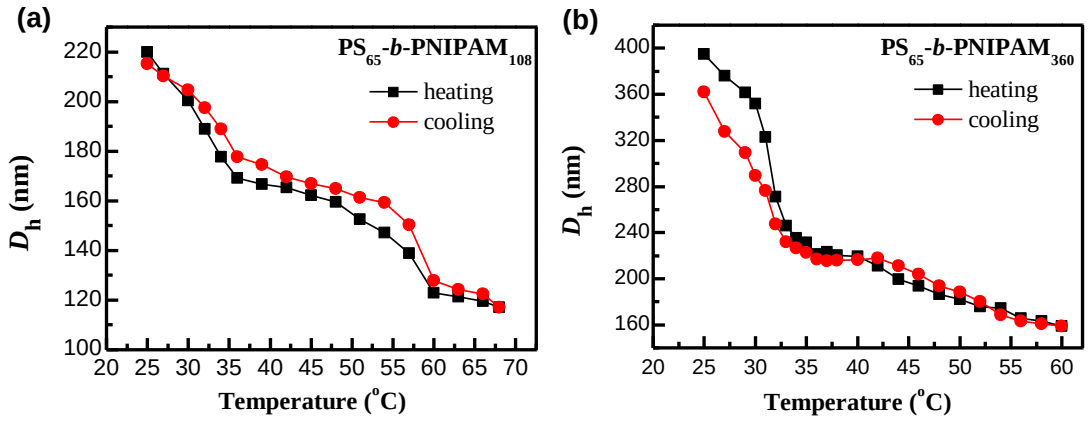

Fig. 1 Temperature dependence of apparent hydrodynamic diameters D_h of PS-*b*-PNIPAM micelles in aqueous solution at a concentration of 0.06 mg/mL. (a) PS_{65}-*b*-$PNIPAM_{108}$; (b) PS_{65}-*b*-$PNIPAM_{360}$.

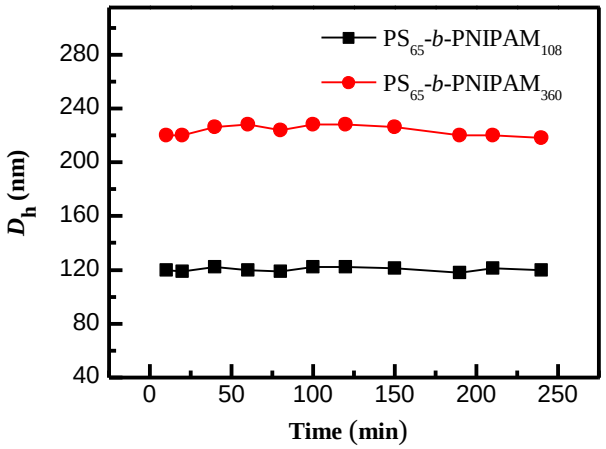

Fig. 2 The apparent hydrodynamic diameters D_h of PS-*b*-PNIPAM micelles as a function of heating time at specified temperatures (60 ℃ for PS_{65}-*b*-$PNIPAM_{108}$ and 40 ℃ for PS_{65}-*b*-$PNIPAM_{360}$).

3.2 Micellar morphologies below and above the LCST

In order to know whether the micellar morphology of PS-*b*-PNIPAM BCPs is altered upon heating, TEM observations were carried out to investigate the micellar morphologies below and above the LCST. The TEM images for the PS_{65}-*b*-$PNIPAM_{108}$ micelles at 25 ℃ and 60 ℃ are shown in Fig. 3. It is observed that the PS_{65}-*b*-$PNIPAM_{108}$ micelles at 25 ℃ exhibit a mixed morphology (Fig. 3a). Most of the micelles are vesicles since the hollow structure can be seen clearly. The average diameter of the vesicles measured by TEM is ~70 nm. The vesicles have a tendency of aggregation to form an interconnected structure. Besides, some spherical micelles are also observed for PS_{65}-*b*-$PNIPAM_{108}$ at 25 ℃. When the temperature of the PS_{65}-*b*-$PNIPAM_{108}$ solution is raised to 60 ℃, the hollow structure of micelles disappears and the micelles become spherical (Fig. 3b), though some of the micelles are still aggregated. The average diameter of the spherical micelles at 60 ℃ is about 62 nm. This shows that the micellar morphologies of PS_{65}-*b*-$PNIPAM_{108}$ in the aqueous solution at 25 ℃ and 60 ℃ are different and heating the solution induces a vesicle-to-sphere transition of the micellar morphology. It should be noted that, only at a temperature well above the LCST of PNIPAM, such as 60 ℃, the micelles of PS_{65}-*b*-$PNIPAM_{108}$ becomes spherical. When the solution temperature is just above the LCST, i.e. 40 ℃, the micelles of PS_{65}-*b*-$PNIPAM_{108}$ are still vesicles (Fig. S4a in supplementary material). This shows that a relatively lower temperature is not enough to induce the transition of the micellar morphology of PS_{65}-*b*-$PNIPAM_{108}$.

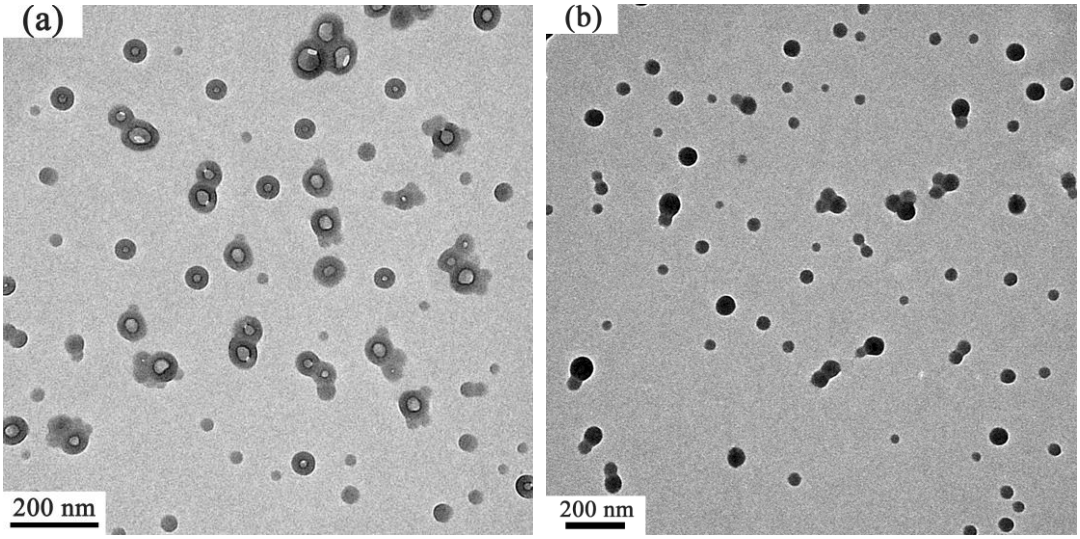

Fig. 3 TEM images of PS_{65}-*b*-$PNIPAM_{108}$ micelles at 25 ℃ (a) and 60 ℃ (b).

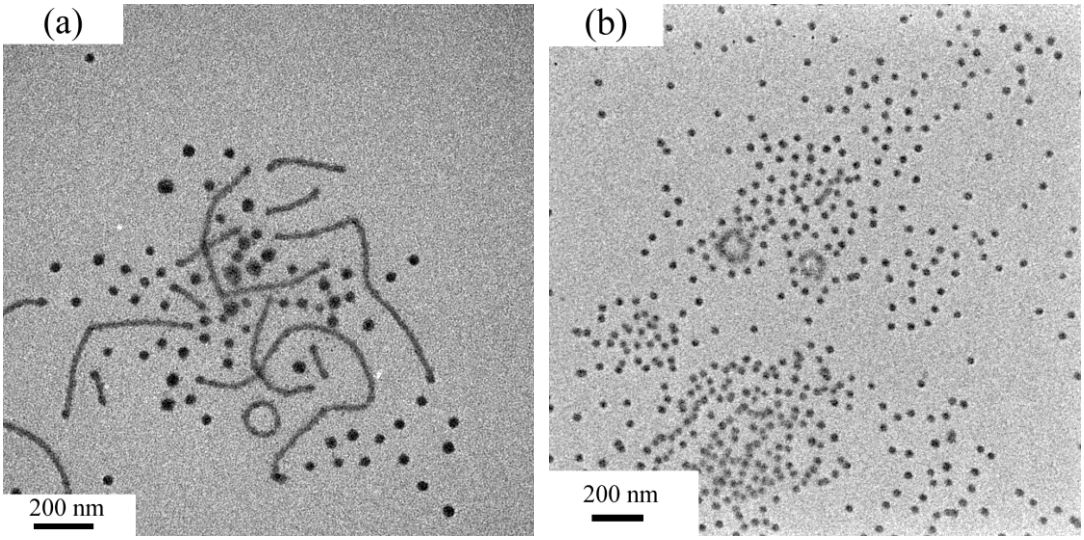

Fig. 4 TEM images of PS_{65}-*b*-$PNIPAM_{360}$ micelles at 25 ℃ (a) and 40 ℃ (b).

Fig. 4 illustrates the TEM images of the micelles prepared from the aqueous solution of PS_{65}-*b*-$PNIPAM_{360}$ at 25 ℃ and 40 ℃, respectively. Mixed cylinders and spheres are observed for the PS_{65}-*b*-$PNIPAM_{360}$ micelles at 25 ℃ (Fig. 4a). The average diameter of the cylindrical and spherical micelles is about 40 nm. By contrast, almost all of the micelles become spherical at 40 ℃ and the average diameter of the micelles is reduced into about 30 nm (Fig. 4b). Further increase of the solution

temperature to 50 ℃, the micelles remain to be spherical (Fig. S4b in supplementary material). This shows that increase in temperature induces the transition of the micellar morphology of PS_{65}-*b*-$PNIPAM_{360}$ as well. It should also be pointed out that the transition of the micellar morphology induced by change of temperature is reversible for both PS_{65}-*b*-$PNIPAM_{108}$ and PS_{65}-*b*-$PNIPAM_{360}$. TEM characterization shows that, when the solutions are cooled from high temperature back to 25 ℃, sphere-to-vesicle and sphere-to-cylinder transitions are observed for micelles of PS_{65}-*b*-$PNIPAM_{108}$ and PS_{65}-*b*-$PNIPAM_{360}$, respectively (Fig. S5 in supplementary material).

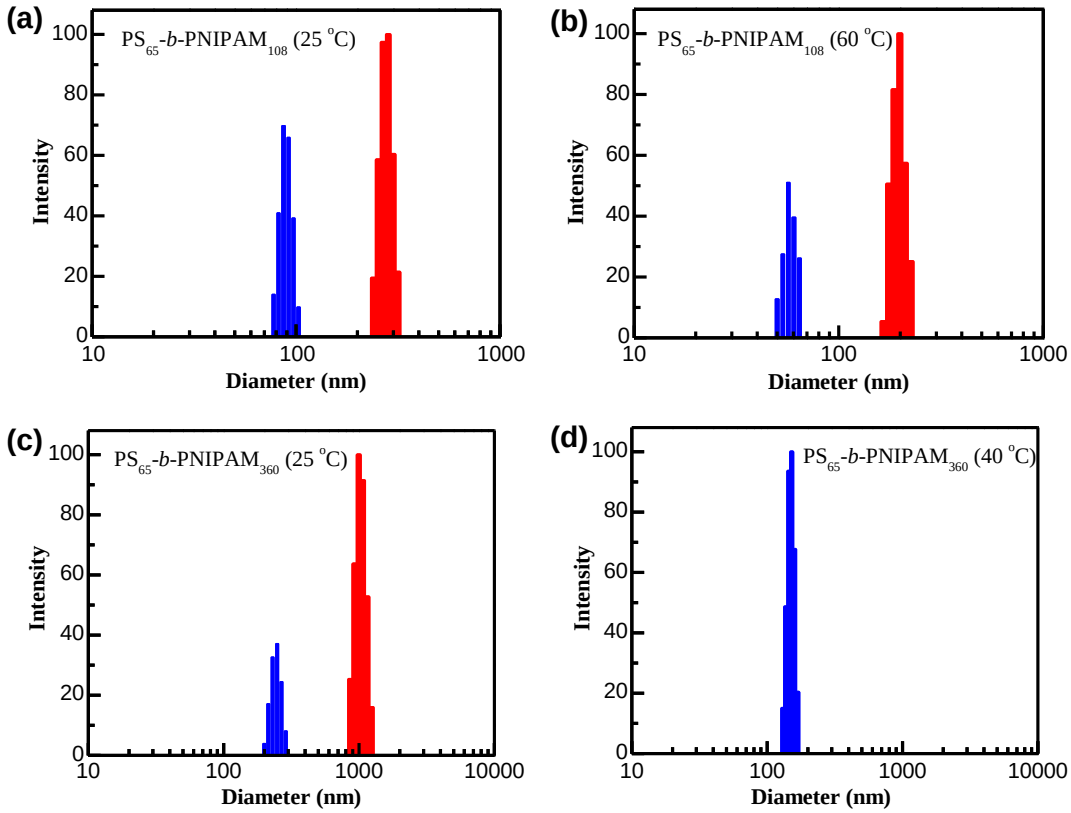

Fig. 5 CONTIN size distributions of PS-*b*-PNIPAM micelles in the aqueous solutions measured at the scattering angle of 90 °. (a) PS_{65}-*b*-$PNIPAM_{108}$ micelles at 25 ℃; (b) PS_{65}-*b*-$PNIPAM_{108}$ micelles at 60 ℃; (c) PS_{65}-*b*-$PNIPAM_{360}$ micelles at 25 ℃; (d) PS_{65}-*b*-$PNIPAM_{360}$ micelles at 40 ℃.

3.3 DLS analysis

The samples for TEM observation are prepared from the dried micelles, though they are frozen during preparation and the observed morphology can reasonably reflect the true micellar morphology in the solutions. The micellar size and the size distribution in the solutions were also studied in-situ using DLS. However, the values of D_h in Figs. 1 and 2 are only mean ones for different populations of micelles, as revealed by TEM. Fig. 5 shows the size distributions of PS_{65}-*b*-$PNIPAM_{108}$ and PS_{65}-*b*-$PNIPAM_{360}$ micelles at different temperatures. A bimodal distribution of the micellar size is observed for PS_{65}-*b*-$PNIPAM_{108}$ micelles at both 25 ℃ and 60 ℃. Combining with the TEM result, the micellar population with a smaller size is assigned to individual vesicles at 25 ℃ and individual spheres at 60 ℃, respectively, while the population of larger size is attributed to the aggregated micelles. Comparing Figs. 5a and 5b, one can see that the size of both populations becomes smaller at elevated temperature. Moreover, the sizes measured by DLS are larger than those observed by TEM. Such a difference is due to solvation of the corona-forming block in the solution, which is frequently reported in literature.

The PS_{65}-*b*-$PNIPAM_{360}$ micelles also exhibit a bimodal size distribution at 25 ℃. This agrees well with the TEM observation and the smaller and larger sizes correspond to the spherical and cylindrical micelles, respectively. The size distribution of the PS_{65}-*b*-$PNIPAM_{360}$ micelles becomes unimodal at 40 ℃. The mean diameters for the spherical micelles of PS_{65}-*b*-$PNIPAM_{360}$ measured by DLS are 237 nm at 25 ℃ and 162 nm at 40 ℃, respectively. The difference between the sizes measured

by DLS and TEM is larger for the PS_{65}-*b*-$PNIPAM_{360}$ micelles than that for the PS_{65}-*b*-$PNIPAM_{108}$ micelles. This is due to the longer PNIPAM block in PS_{65}-*b*-$PNIPAM_{360}$.

One drawback of DLS is that the micellar morphology cannot be identified directly. Nevertheless, DLS can differentiate the isotropic spherical particles from the anisotropic ones based on the angular dependence of the scattering property of the particles. As a result, DLS measurements were carried out at different scattering angles and the electric-field autocorrelation functions, $g^{(1)}(t)$, were obtained (Fig. S6 in supplementary material). However, both TEM and DLS characterizations reveal that there are two populations of micelles in the PS_{65}-*b*-$PNIPAM_{108}$ solutions at 25 ℃ and 60 ℃ and in the PS_{65}-*b*-$PNIPAM_{360}$ solution at 25 ℃. Since the larger particles usually exhibit a longer relaxation time and the smaller particles have a shorter relaxation time, a stretched exponential function can be used to describe the electric-field autocorrelation function of the system with two relaxation modes:[49,50]

$$g^{(1)}(t) = A_{fast}\exp\left(-\frac{t}{\tau_{fast}}\right) + A_{slow}\exp\left[-\left(\frac{t}{\tau_{slow}}\right)^{\gamma}\right] \qquad (1)$$

Where τ_{fast} and τ_{slow} are the relaxation times of the fast and slow modes, respectively. The reciprocal of τ is the relaxation rate, Γ. The stretched exponent, γ, ($0 < \gamma \leq 1$) is inversely proportional to the width of the distribution of relaxation time. A smaller value of γ implies a broader distribution of the relaxation time. The pre-factors A_{fast} and A_{slow} are the amplitudes of the fast and slow relaxation modes, respectively, and the sum of A_{fast} and A_{slow} is close to 1.

On the other hand, when there is only one population of spherical particles in the

solution, the electric-field autocorrelation function $g^{(1)}(t)$ can be fitted with a second-order cumulant expansion method:[51]

$$g^{(1)}(t) = A\exp(-\Gamma t)(1+\mu_2 t^2/2!+\cdots) \quad (2)$$

Where μ_2 is the second cumulant, Γ is the relaxation rate, which is reciprocal of relaxation time ($1/\tau$). The parameter γ in Eq.(1) is equal to μ_2/Γ^2 here.

In the present work, the electric-field autocorrelation functions of the PS_{65}-*b*-$PNIPAM_{108}$ solutions at 25 ℃ and 60 ℃ and the PS_{65}-*b*-$PNIPAM_{360}$ solution at 25 ℃ are fitted with Eq.(1), whereas the electric-field autocorrelation function of the PS_{65}-*b*-$PNIPAM_{360}$ solution at 40 ℃ is fitted with Eq.(2). The parameters obtained by fitting the electric-field autocorrelation functions at the scattering angle of 90 ° are summarized in Table 2.

Table 2 The parameters obtained by fitting $g^{(1)}(t)$ of PS-*b*-PNIPAM solutions at the scattering angle of 90 °.

Sample	PS_{65}-*b*-$PNIPAM_{108}$		PS_{65}-*b*-$PNIPAM_{360}$	
temperature	25 ℃	60 ℃	25 ℃	40 ℃[a]
τ_{fast} (ms)	0.73	0.46	0.73	0.47
τ_{slow} (ms)	3.72	1.57	4.24	-
A_{fast}	0.69	0.62	0.37	1
A_{slow}	0.31	0.38	0.63	-
γ	0.56	0.26	0.65	0.12

[a]For PS_{65}-*b*-$PNIPAM_{360}$ at 40 ℃, A_{fast} τ_{fast} and γ correspond to the A, $1/\Gamma$, and μ_2/Γ^2 in Eq.(2).

So far, there still exist controversies about the assignments of the fast and the slow relaxation modes in the DLS characterization of micelle solution. They may be assigned to the movements of different populations of particles with different sizes, or

to the different motion modes of single population of anisotropic particles.[52-57] Here we believe that τ_{fast} and τ_{slow} correspond to the relaxation times of smaller and larger micelles, respectively, which are individual micelles and aggregated micelles in the PS_{65}-*b*-$PNIPAM_{108}$ solution at 25 ℃ and 60 ℃ or spherical and cylindrical micelles in the PS_{65}-*b*-$PNIPAM_{360}$ solution at 25 ℃.

It can be seen from Table 2 that the values of τ_{fast} and τ_{slow} at 60 ℃ are much smaller than those at 25 ℃ for the PS_{65}-*b*-$PNIPAM_{108}$ solution, but the values of the pre-factors A_{fast} and A_{slow} are nearly the same at 25 ℃ and 60 ℃. This shows that the vesicle-to-sphere transition leads to decrease in the size of two populations of micelles, but the fractions of the aggregated and individual micelles almost remain the same. As for the PS_{65}-*b*-$PNIPAM_{360}$ solution, the pre-factor A_{fast} is 0.37 at 25 ℃. This indicates that the cylindrical micelles are the majority, which is in accordance with the TEM observation. Moreover, both the values of τ_{fast} and γ are smaller at 40 ℃ than those at 25 ℃ for the PS_{65}-*b*-$PNIPAM_{360}$ solution. This indicates a smaller size and a narrower size distribution of the micelles resulting from the cylinder-to-sphere transition, which agrees with the TEM result as well.

The yielded Γ_{fast} and Γ_{slow} at various scattering angles, which are the reciprocals of τ_{fast} and τ_{slow}, respectively, are plotted against q^2, as shown in Figs. 6 and 7. One can see that, there is linear relationship between Γ_{fast} and q^2 for both solutions, irrespective of the temperature (Figs. 6a and 7a). This implies that Γ_{fast} corresponds to the relaxation rate of an isotropic movement,[54] and this result also supports our assignment of Γ_{fast} to spherical vesicles or spheres. By contrast, no linear relationship

is observed between Γ_{slow} and q^2 for the PS_{65}-*b*-$PNIPAM_{108}$ solution at 25 ℃ and 60 ℃ and the PS_{65}-*b*-$PNIPAM_{360}$ solution at 25 ℃ (Figs. 6b and 7b), indicating the anisotropic shape of the micelles. Fitting of the electric-field autocorrelation functions shows that isotropic spherical micelles and anisotropic micelles co-exist in PS_{65}-*b*-$PNIPAM_{108}$ solution at 25 ℃ and 60 ℃ and the PS_{65}-*b*-$PNIPAM_{360}$ solution at 25 ℃, whereas there exist only spherical micelles in PS_{65}-*b*-$PNIPAM_{360}$ solution at 40 ℃. This finding is in accordance with the TEM observations.

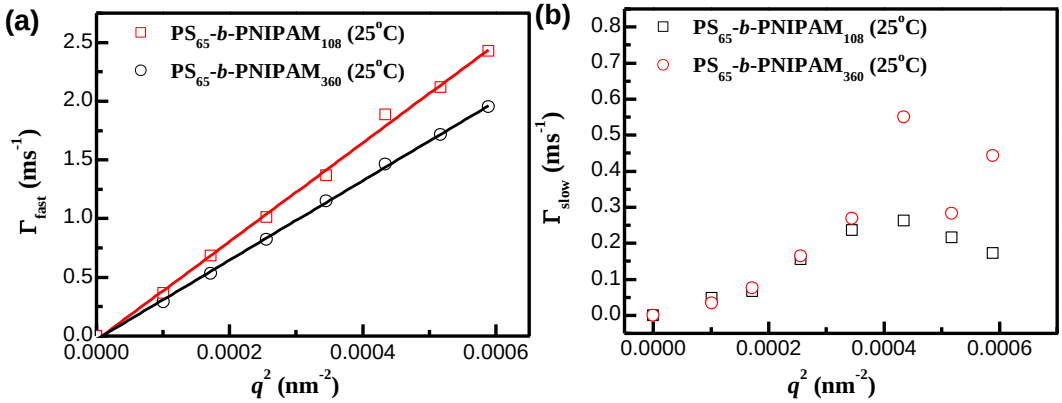

Fig. 6 Plots of Γ_{fast} (a) and Γ_{slow} (b) versus q^2 for the PS-*b*-PNIPAM solutions at 25 ℃.

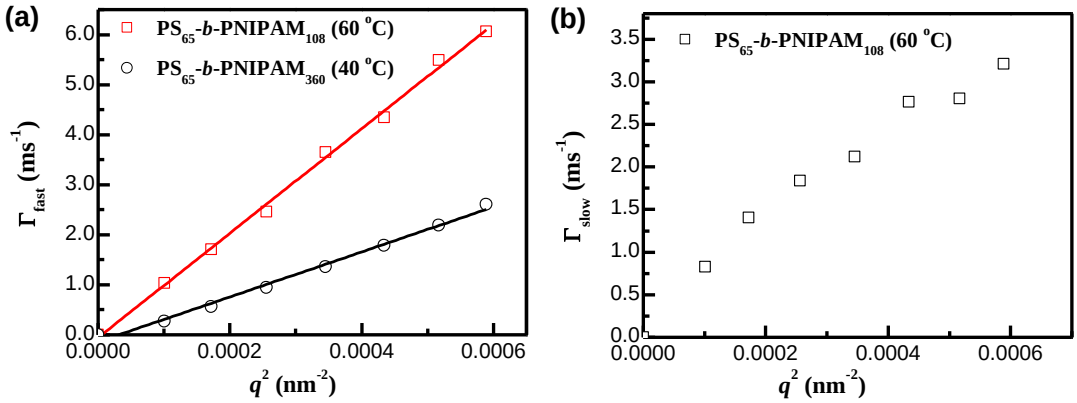

Fig. 7 Plots of Γ_{fast} (a) and Γ_{slow} (b) versus q^2 for the PS-*b*-PNIPAM solutions at the elevated temperatures. For PS_{65}-*b*-$PNIPAM_{360}$ solution at 40 ℃, Γ_{fast} corresponds to Γ in Eq.(2).

3.4 Possible mechanism for the transitions of micellar morphology

The TEM and DLS results show that the micellar morphologies are different at lower and higher temperatures for both the PS_{65}-*b*-$PNIPAM_{108}$ and PS_{65}-*b*-$PNIPAM_{360}$ solutions. Raising temperature induces a vesicle-to-sphere transition for the PS_{65}-*b*-$PNIPAM_{108}$ micelles and a cylinder-to-sphere transition for the PS_{65}-*b*-$PNIPAM_{360}$ micelles. In order to understand the driving force of the morphological transition, the free energy of the micelles was analyzed. Because the free energy of the core, F_{core}, usually plays a minor role, thus this item of free energy is neglected, and only F_{corona} and $F_{interface}$ are considered.[15,58,59] The free energy of micellar corona, F_{corona}, can be expressed as:[17]

$$F_{corona} / kT = C_H C_F N (sa^{-2})^{-1/2\nu} \quad (3)$$

Where $\hat{C}_H$ and $\hat{C}_F$ are numerical coefficients, N is the polymerization degree of the PNIPAM block, s is the area occupied by per PNIPAM chain at the interface between the corona and core of the micelles, a is the length of a NIPAM unit, and ν is the scaling exponent with a value of 3/5 in the good solvent or 1/2 in the θ solvent.

In the good solvent, $\hat{C}_H$ and $\hat{C}_F$ can be expressed as:

$$C_H = C_H (l / a)^{1/3} \upsilon^{1/3} \quad (4)$$

$$C_F = C_F \quad (5)$$

Where C_H and C_F are constants with values of 0.68 and 1.83, respectively, l is the Kuhn length of PNIPAM and υ is the excluded volume of PNIPAM in a specific solvent.

The interfacial free energy, $F_{interface}$, also contributes to the total free energy for

star-like micelles. $F_{interface}$ can be expressed as:

$$F_{interface} = \gamma s \qquad (6)$$

Where γ is the surface tension between the PS core and the solvent water.

Since both F_{corona} and $F_{interface}$ are related to *s*, the value of *s* should be determined firstly. The value of *s* for micelles of different shapes can be calculated as follows:[17]

$$s_{sphere} = 3V_{PS}N_{PS} / (fR_{core}) \qquad (7)$$

$$s_{cylinder} = 2V_{PS}N_{PS} / (fR_{core}) \qquad (8)$$

$$s_{vesicle} = V_{PS}N_{PS} / (fR_{core}) \qquad (9)$$

Where V_{PS} is the volume of a styrene unit, N_{PS} is the polymerization degree of PS, *f* is the swelling degree of the PS core by the solvent water (here f = 1), and R_{core} is the radius of the core in the spherical and cylindrical micelles or the half thickness of the PS layer in the vesicular micelles.

The values of R_{core} can be estimated from the TEM images. At low temperature, we assume that the observed images only correspond to the PS blocks and the corona formed by the PNIPAM blocks cannot be discerned by TEM due to the low electron density. By contrast, at high temperature both the PS and PNIPAM blocks contribute to radius of the observed micelles (R) because of collapse of the PNIPAM block, thus R_{core} is calculated from R measured by TEM and the volume fraction of PS block. The calculated values of *s* are summarized in Table 3. It is observed that the area occupied by per chain at the interface is about 1 ~ 2 nm^2 at 25 °C. Zhang et al. determined the core radius of the spherical PS_{207}-*b*-$PNIPAM_{357}$ micelles at room temperature to be 61 nm.[31] The calculated s based on our method is 1.94 nm^2, which is comparable to the

value for spherical micelles of PS_{65}-*b*-$PNIPAM_{360}$ in Table 3. It is also noticed that, for the same PS-b-PNIPAM, the value of *s* in the spherical micelles is larger than that in the cylindrical or vesicular ones. When heated above the LCST, the value of *s* becomes larger.

The aggregation number (N_{agg}) in the micelles can be further calculated based on the area occupied by per chain and the micelle size, which is also given in Table 3. One can see that, at 25 °C the spherical micelles contain fewer BCP chains than the cylindrical or vesicular ones for the same PS-*b*-PNIPAM BCP. After morphological transition at higher temperature, the aggregation number becomes significantly smaller.

Table 3 The estimated values of the area occupied by per PNIPAM chain (*s*) and the aggregation number (N_{agg}) in the PS-*b*-PNIPAM micelles.

Samples	25 °C			60 °C (or 40 °C)		
	morphology	*s* (nm^2)	N_{agg}	morphology	*s* (nm^2)	N_{agg}
PS_{65}-*b*-$PNIPAM_{108}$	vesicle	1.23	4170	sphere	3.02	630
	sphere	1.80	2970			
PS_{65}-*b*-$PNIPAM_{360}$	cylinder	1.54	47330	sphere	4.38	210
	sphere	1.90	2550			

Firstly we analyze the free energies of PS_{65}-*b*-$PNIPAM_{108}$ and PS_{65}-*b*-$PNIPAM_{360}$ at 25 °C. The data in Table 3 shows there is a difference of 46% in the value of *s* between the vesicular and spherical micelles of PS_{65}-*b*-$PNIPAM_{108}$, whereas the difference is only 23% for the cylindrical and spherical micelles of PS_{65}-*b*-$PNIPAM_{360}$. This indicates that there is a smaller difference in $F_{interface}$ between the cylindrical and

spherical micelles of PS_{65}-*b*-$PNIPAM_{360}$, since the surface tension (γ) is the same for different micellar morphologies at a given temperature. Therefore, F_{corona} is the predominant free energy for the micellar morphology of PS_{65}-*b*-$PNIPAM_{360}$. Although the difference in *s* between different micellar morphologies is smaller, the higher polymerization degree (*N*) in PS_{65}-*b*-$PNIPAM_{360}$ can enlarge such a difference, leading to more evident difference in F_{corona} between the cylindrical and spherical micelles. Since a larger *s* results in a smaller F_{corona} (Eq.(3)), a spherical morphology is favorable for PS_{65}-*b*-$PNIPAM_{360}$. However, due to the small difference in *s*, cylindrical micelles can be formed as well. By contrast, for PS_{65}-*b*-$PNIPAM_{108}$ micelles, the $F_{interface}$ should play a major role because of the shorter PNIPAM block and the larger difference in *s* between different micellar morphologies. As a result, vesicles tend to be formed for PS_{65}-*b*-$PNIPAM_{108}$ because of the smaller *s* and $F_{interface}$. Above theoretical analysis agrees with the TEM and DLS results. The detailed calculations of free energies for PS_{65}-*b*-$PNIPAM_{360}$ and PS_{65}-*b*-$PNIPAM_{108}$ micelles at 25 °C are given in supplementary material. Therefore, the micellar morphologies of PS_{65}-*b*-$PNIPAM_{108}$ and PS_{65}-*b*-$PNIPAM_{360}$ at 25 °C can be interpreted in terms of free energy of the micelles.

Next we will discuss the free energy of the PS-*b*-PNIPAM micelles at elevated temperature. When the temperature rises above the LCST of PNIPAM, F_{corona} of the micelles cannot be discussed due to inapplicability of Eqs.(3) and (4) in the poor solvent. However, because the PNIPAM blocks are collapsed into globules, the size of the corona is greatly reduced, leading to formation of "crew-cut" micelles. If only the

overall size of the PNIPAM blocks is considered, the repulsion force among different PNIPAM blocks should be much smaller than that at 25 °C and F_{corona} may be ignored, which is usually the case in other "crew-cut" micelles. On the other hand, $F_{interface}$ of the cylindrical or vesicular micelles is smaller than that of the spherical ones, since *s* is the largest in the spherical micelles for the same BCPs. As a result, cylindrical or vesicular micelles, instead of spherical ones, tend to be formed at elevated temperatures for PS-*b*-PNIPAM. Unfortunately, such a prediction by qualitative analysis of free energy is opposed to the experimental observation.

Temperature-induced morphological transitions of BCP micelles have been reported by different groups. Usually, when the solubility of the corona-forming block is enhanced, spherical micelles are formed at an elevated temperature. For example, a cylinder-to-sphere transition was observed by Abbas for polystyrene-*b*-poly(dimethyl siloxane) (PS-*b*-PDMS) in dibutyl phthalate (selective for PS) as temperature was raised.[60] Cheng reported that both PEO_{827}-*b*-PS_{164} in dioxane/cyclohexane (selective for PS) and PS_{962}-*b*-PEO_{227} in DMF/water (selective for PEO) underwent a morphological transition of vesicles → cylinders → spheres upon increasing the temperature.[61, 62] LaRue demonstrated the polystyrene-*b*-polyisoprene (PS-*b*-PI) micelles in heptane (selective for PS) changed from cylinders to spheres during heating the solution.[63] By contrast, when the corona-forming block has a strong favorable interaction (such as hydrogen bonding) with the solvent and such an interaction is weakened at elevated temperatures, a sphere-to-cylinder or sphere-to-vesicles transition is frequently observed as temperature increases. For

instance, a sphere-to-cylinder transition usually occurs for poly(ethylene oxide)-poly(propylene oxide)-poly(ethylene oxide) (PEO-*b*-PPO-*b*-PEO) in water when the micellar solution is heated.[64,65] As temperature rose, sphere-to-cylinder, sphere-to-vesicle and sphere-to-tubule transitions were observed in the aqueous solutions of monomethoxy-poly(ethylene glycol)-*b*-poly(trimethylene carbonate),[66] monomethoxy poly(ethylene glycol)-poly(ε-caprolactone)-polyphosphoester 3-miktoarm star terpolymer,[67] poly(ethylene glycol)-*b*-poly(*N*-isopropylacrylamide) -*b*-poly(isoprene),[38] and poly(t-butyl acrylate)-*b*-poly(*N*-isopropylacrylamide) and poly(methyl acrylate)-*b*-poly(*N*-isopropylacrylamide) with a charged hydrophilic head group,[39, 40] respectively. These results can be explained in terms of free energy of the micelles. When the corona-forming blocks are less solvated, the sphere-to-cylinder or sphere-to-vesicle transition can be observed. In the present work, the PNIPAM blocks become less soluble above the LCST, but cylinder-to-sphere and vesicle-to-sphere transitions occur, which are different from most of the results reported in literature.

Since our result cannot be explained from $F_{interface}$, F_{corona} must still play an important role in determining the micellar morphology at elevated temperature. We notice that the values of *s* at high temperatures are larger than those at 25 °C for both PS-*b*-PNIPAM BCPs (Table 3), though these values are not accurate. This is out of our expectation, since the PNIPAM blocks are collapsed and have a smaller overall size above the LCST and thus should occupy smaller area. The larger values of *s* imply that the PNIPAM blocks are more crowded at elevated temperature and this is responsible for the formation of the spherical micelles.

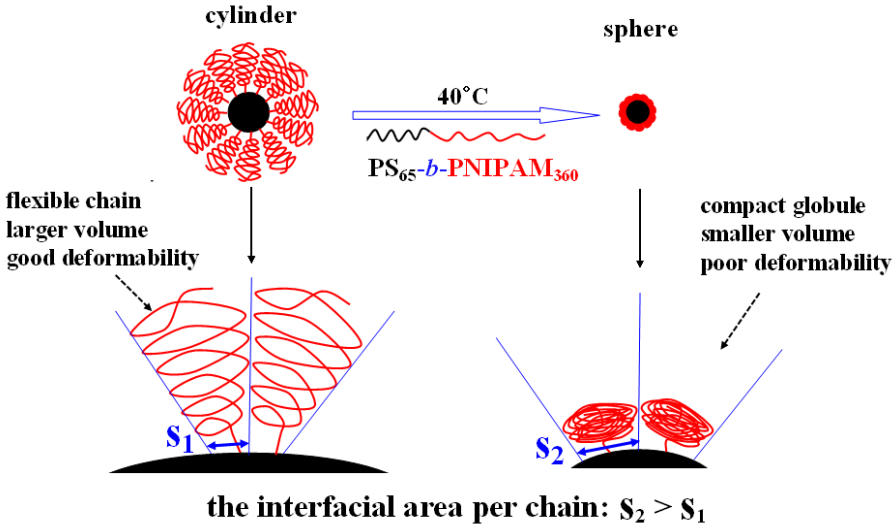

Scheme 2 Schematic illustration for the cylinder-to-sphere transition of the PS_{65}-*b*-$PNIPAM_{360}$ micelles upon heating.

Nevertheless, why do the PNIPAM blocks occupy larger area after collapse at high temperature? In order to explain this phenomenon, we propose that the concept of local deformability. The calculation of F_{corona} in Eq.(3) is based on an overall parameter, the excluded volume. However, the excluded volume cannot reflect the local conformation of PNIPAM chains at different positions inside the micelles. When the temperature is lower than the LCST, the deformation of the flexible PNIPAM chain grafted on a curved interface varies with the distance to the interface (Scheme 1). As temperature rises, the excluded volume of PNIPAM becomes smaller. At the same time, the collapsed PNIPAM globules become more compact as well and thus the deformability of PNIPAM is reduced. As a result, at the interface of the corona and core in the micelles, a collapsed PNIPAM globule occupies larger area than single flexible PNIPAM chain, though the total volume of the globule is smaller than that of the flexible chain.

The local deformability and the area occupied by per PNIPAM chain in the PS_{65}-*b*-$PNIPAM_{360}$ micelles at low and high temperatures can be schematically depicted in Scheme 2. Since in the cylindrical micelles the area occupied by per PNIPAM chain is usually smaller than that in the spherical micelles, the compact globules would become more repulsive due to their weaker deformability and F_{corona} would increase dramatically, if cylindrical micelles were formed at the temperature above the LCST. In order to reduce F_{corona} at high temperatures, cylinder-to-sphere transition occurs for the PS_{65}-*b*-$PNIPAM_{360}$ micelles. The vesicle-to-sphere transition of the PS_{65}-*b*-$PNIPAM_{108}$ micelles upon heating can be explained in a similar way. One may argue that the change of enthalpy due to the breakdown of hydrogen bonds between PNIPAM and H_2O upon raising temperature is main contribution to the morphological transition of the PS-*b*-PNIPAM micelles. Indeed, the interaction of the corona-forming block with the solvent has been taken into account in calculation of F_{corona}, in which the excluded volume of the corona-forming block is determined by both enthalpy and entropy (see calculation of free energy of micelles at 25 °C in supplementary material).

One can see that, the vesicle-to-sphere and cylinder-to-sphere transitions for the PS-*b*-PNIPAM BCPs upon raising temperature observed here can be reasonably interpreted by taking the local deformability of corona chains into account. However, it should be noted that the micellar morphologies of the PS-*b*-PNIPAM BCPs in the present work are different from those reported in literature to some extent. For example, spherical micelles were reported for PS_{207}-*b*-$PNIPAM_{357}$ and

PS_{77}-*b*-$PNIPAM_{120}$ at room temperature.[31,47] The block ratios of [NIPAM]/[S] in these two BCPs are 1.72 and 1.56, which are similar to that in PS_{65}-*b*-$PNIPAM_{108}$ ([NIPAM]/[S]=1.66). Vesicles were only observed for PS_{207}-*b*-$PNIPAM_{176}$ with a much smaller block ratio ([NIPAM]/[S] = 0.85).[31] Moreover, temperature-induced transitions of the micellar morphology are rarely reported for the PS-*b*-PNIPAM BCPs.[31, 47, 68] These differences may originate from the different preparation methods of the micellar solutions. In literature, a certain amount of water was slowly added into the homogeneous organic solution containing the PS-*b*-PNIPAM BCP prior to dialysis.[31,47,68] By contrast, in the present work the PS-*b*-PNIPAM solutions were directly dialyzed against water. As shown by the calculation, the difference in the free energy between the micelles of different morphologies at 25 °C indeed is not quite large. This means that different micellar morphologies are probably formed, depending on the preparation method. Such a phenomenon is frequently reported in literature.[69-72] When the PS-*b*-PNIPAM solution in THF is directly dialyzed against water, the solvent composition changes greatly in the initial dialysis stage due to the large difference in solvent composition inside and outside the dialysis tube, but just changes slowly in the final stage. As a result, the driving force for formation of micelles or transition of micellar morphology becomes weaker gradually in the progress of dialysis, leading to formation of different micelles. In order to verify the effect of preparation method, the aqueous micellar solution of PS_{65}-*b*-$PNIPAM_{108}$ was also prepared according to the procedure reported in literature.[47] The micellar morphology of PS_{65}-*b*-$PNIPAM_{108}$ at 25 °C, which is prepared by addition of water

into the DMF solution followed by dialysis, is spherical and no vesicles are observed (Fig. S7a in supplementary material). When water is slowly added into the organic solution to form micelles before dialysis, equilibrium is nearly approached in each step during addition of water and thus only one type of micelles with local minimal free energy is formed. Because of the spherical morphology at 25 °C, the collapsed PNIPAM block will become more crowded at 60 °C, as we predict, thus the micelles are still spherical at 60 °C and no morphological transition can be observed (Fig. S7b in supplementary material). After the PS_{65}-*b*-$PNIPAM_{108}$ micelles prepared from the DMF solution are cooled back to 25 °C from 60 °C, no morphology transition is observed either (Fig. S7c in supplementary material).

It should also be pointed out that the local deformability of the PNIPAM block may exert its effect on morphological transition of the micelles only in a suitable range of block length, which cannot be accurately predicted so far. When the PNIPAM block is too long relative to the core-forming block, the PNIAPM chains in the micelles are crowded at both the temperatures below and above the LCST, thus spherical micelles are always formed and no morphological transition is observed. On the other hand, if the PNIPAM block is too short, such as in the crew-cut micelles, the collapsed globules formed above the LCST are not crowded due to their small size, thus no morphological transition or vesicle-to-sphere, instead of sphere-to-vesicle, is observed upon heating, as reported in literature.[38-40]

4 Conclusions

The TEM and DLS results show that reversible morphological transitions takes place for two PS-*b*-PNIPAM BCPs in aqueous solution solely by changing the temperature. Upon raising temperature, the morphology changes from vesicles to spheres for the PS_{65}-*b*-$PNIPAM_{108}$ micelles and from cylinders to spheres for the PS_{65}-*b*-$PNIPAM_{360}$ micelles. Such transitions are opposed to the theoretical prediction when only the overall volume change is taken into account. We proposed that the local deformability of the PNIPAM chains varies with temperature. At the temperature above the LCST, the compact globules exhibit weaker local deformability and occupy larger area than the flexible chains below the LCST. Therefore, the globules are more crowded and spherical micelles tend to be formed at elevated temperature.

Acknowledgements

This work was supported by the National Natural Science Foundation of China (21274130 and 20974099).

References

1. M. Wilhelm, C. L. Zhao, Y. C. Wang, R. L. Xu, M. A. Winnik, J. L. Mura, G. Riess and M. D. Croucher, *Macromolecules*, 1991, **24**, 1033-1040.
2. G. Riess, *Prog. Polym. Sci.*, 2003, **28**, 1107-1170.
3. A. Halperin, M. Tirrell and T. P. Lodge, *Adv. Polym. Sci.*, 1992, **100**, 31-71.
4. L. F. Zhang and A. Eisenberg, *Polym. Adv. Technol.*, 1998, **9**, 677-699.
5. L. F. Zhang and A. Eisenberg, *J. Am. Chem. Soc.*, 1996, **118**, 3168-3181.
6. S. Förster and M. Antonietti, *Adv. Mater.*, 1998, **10**, 195-217.
7. H. W. Shen and A. Eisenberg, *J. Phys. Chem. B*, 1999, **103**, 9473-9487.
8. F. T. Liu and A. Eisenberg, *J. Am. Chem. Soc.*, 2003, **125**, 15059-15064.
9. Z. L. Zhou, Z. B. Li, Y. Ren, M. A. Hillmyer and T. P. Lodge, *J. Am. Chem. Soc.*, 2003, **125**, 10182-10183.
10. J. Bang, S. M. Jain, Z. B. Li, T. P. Lodge, J. S. Pedersen, E. Kesselman and Y. Talmon, *Macromolecules*, 2006, **39**, 1199-1208.
11. R. C. Hayward and D. J. Pochan, *Macromolecules*, 2010, **43**, 3577-3584.
12. W. D. He, X. L. Sun, W. M. Wan and C. Y. Pan, *Macromolecules*, 2011, **44**, 3358-3365.
13. W. N. He and J. T. Xu, *Prog. Polym. Sci.*, 2012, **37**, 1350-1400.
14. A. Halperin, *Macromolecules*, 1987, **20**, 2943-2946.
15. O. V. Borisov and E. B. Zhulina, *Macromolecules*, 2002, **35**, 4472-4480.
16. L. Chen, H. W. Shen and A. Eisenberg, *J. Phys. Chem. B*, 1999, **103**, 9488-9497.
17. E. B. Zhulina, M. Adam, I. LaRue, S. S. Sheiko and M. Rubinstein,

Macromolecules, 2005, **38**, 5330-5351.

18. F. B. Zhao, J. P. Sun, Z. L. Liu, L. Feng and J. W. Hu, *J. Polym. Sci. Part B: Polym. Phys.*, 2010, **48**, 364-371.
19. F. M. Winnik, *Macromolecules*, 1990, **23**, 233-242.
20. S. Fujishige, K. Kubota and I. Ando, *J. Phys. Chem.*, 1989, **93**, 3311-3313.
21. C. Wu and S. Q. Zhou, *Macromolecules*, 1995, **28**, 8381-8387.
22. X. H. Wang, X. P. Qiu and C. Wu, *Macromolecules*, 1998, **31**, 2972-2976.
23. I. Dimitrov, B. Trzebicka, A. H. E. Muller, A. Dworak and C. B. Tsvetanov, *Prog. Polym. Sci.*, 2007, **32**, 1275-1343.
24. H. Wei, S. X. Cheng, X. Z. Zhang and R. X. Zhuo, *Prog. Polym. Sci.*, 2009, **34**, 893-910.
25. M. Motornov, Y. Roiter, I. Tokarev and S. Minko, *Prog. Polym. Sci.*, 2010, **35**, 174-211.
26. A. X. Mei, X. L. Guo, Y. W. Ding, X. H. Zhang, J. T. Xu, Z. Q. Fan and B. Y. Du, *Macromolecules*, 2010, **43**, 7312-7320.
27. Y. P. Lu, T. Q. Chen, A. X. Mei, T. Y. Chen, Y. W. Ding, X. H. Zhang, J. T. Xu, Z. Q. Fan and B. Y. Du, *Phys. Chem. Chem. Phys.*, 2013, **15**, 8276-8286.
28. B. Y. Du, A. X. Mei, Y. Yang, Q. F. Zhang, Q. Wang, J. T. Xu and Z. Q. Fan, *Polymer*, 2010, **51**, 3493-3502.
29. Y. P. Lu, X. H. Zhang, Z. Q. Fan and B. Y. Du, *Polymer*, 2012, **53**, 3791-3801.
30. T. Q. Chen, Y. P. Lu, T. Y. Chen, X. H. Zhang and B. Y. Du, *Phys. Chem. Chem. Phys.*, 2014, **16**, 5536-5544.

31. W. A. Zhang, X. C. Zhou, H. Li, Y. Fang and G. Z. Zhang, *Macromolecules*, 2005, **38**, 909-914.

32. T. Tang, V. Castelletto, P. Parras, I. W. Hamley, S. M. King, D. Roy, S. Perrier, R. Hoogenboom and U. S. Schubert, *Macromol. Chem. Phys.*, 2006, **207**, 1718-1726.

33. X. J. Loh, Z. X. Zhang, Y. L. Wu, T. S. Lee and J. Li, *Macromolecules*, 2009, **42**, 194-202.

34. J. Adelsberger, E. Metwalli, A. Diethert, I. Grillo, A. M. Bivigou-Koumba, A. Laschewsky, P. Muller-Buschbaum and C. M. Papadakis, *Macromol. Rapid Commun.*, 2012, **33**, 254-259.

35. J. Qian and F. P. Wu, *Macromolecules*, 2008, **41**, 8921-8926.

36. S. Kessel, C. N. Urbani and M. J. Monteiro, *Angew. Chem. Int. Ed.*, 2011, **50**, 8082-8085.

37. S. Kessel, N. P. Truong, Z. F. Jia and M. J. Monteiro, *J. Polym. Sci. Part A: Polym. Chem.*, 2012, **50**, 4879-4887.

38. A. Sundararaman, T. Stephan and R. B. Grubbs, *J. Am. Chem. Soc.*, 2008, **130**, 12264-12265.

39. A. O. Moughton and R. K. O'Reilly, *Chem. Commun.*, 2010, **46**, 1091-1093.

40. A. O. Moughton, J. P. Patterson and R. K. O'Reilly, *Chem. Commun.*, 2011, **47**, 355-357.

41. J. T. Lai, D. Filla and R. Shea, *Macromolecules*, 2002, **35**, 6754-6756.

42. K. Cao, J. T. Xu and X. S. Wang, *Chin. J. Polym. Sci.*, 2012, **30**, 674-681.

43. J. Shan, J. Chen, M. Nuopponen and H. Tenhu, *Langmuir*, 2004, **20**, 4671-4676.

44. T. Wu, Y. F. Zhang, X. F. Wang and S. Y. Liu, *Chem. Mater.*, 2008, **20**, 101-109.

45. Z. Cao, B. Y. Du, T. Y. Chen, H. T. Li, J. T. Xu and Z. Q. Fan, *Langmuir*, 2008, **24**, 5543-5551.

46. F. Kohori, K. Sakai, T. Aoyagi, M. Yokoyama, Y. Sakurai and T. Okano, *J. Control. Release*, 1998, **55**, 87-98.

47. M. Nuopponen, J. Ojala and H. Tenhu, *Polymer*, 2004, **45**, 3643-3650.

48. Y. F. Hu, V. Darcos, S. Monge and S. M. Li, *J. Polym. Sci. Part A: Polym. Chem.*, 2013, **51**, 3274-3283.

49. B. Nystrom, H. Walderhaug and F. K. Hansen, *J. Phys. Chem.*, 1993, **97**, 7743-7752.

50. K. L. Ngai, *Adv. Colloid Interf. Sci.*, 1996, **64**, 1-43.

51. B. Chu, *Laser Light Scattering*, Academic, New York, 1991.

52. D. Lehner, H. Lindner and O. Glatter, *Langmuir*, 2000, **16**, 1689-1695.

53. G. Guerin, J. Raez, I. Manners and M. A. Winnik, *Macromolecules*, 2005, **38**, 7819-7827.

54. H. Y. Huang, R. Hoogenboom, M. A. M. Leenen, P. Guillet, A. M. Jonas, U. S. Schubert and J. F. Gohy, *J. Am. Chem. Soc.*, 2006, **128**, 3784-3788.

55. B. Y. Du, A. X. Mei, K. Z. Yin, Q. F. Zhang, J. T. Xu and Z. Q. Fan, *Macromolecules*, 2009, **42**, 8477-8484.

56. W. N. He, J. T. Xu, B. Y. Du, Z. Q. Fan and X. S. Wang, *Macromol. Chem. Phys.*, 2010, **211**, 1909-1916.

57. W. N. He, J. T. Xu, B. Y. Du and Z. Q. Fan, *Macromol. Chem. Phys.*, 2012, **213**, 952-964.

58. P. Bhargava, J. X. Zheng, P. Li, R. P. Quirk, F. W. Harris and S. Z. D. Cheng, *Macromolecules*, 2006, **39**, 4880-4888.

59. G. V. Jensen, Q. Shi, G. R. Deen, K. Almdal and J. S. Pedersen, *Macromolecules*, 2012, **45**, 430-440.

60. S. Abbas, Z. B. Li, H. Hassan and T. P. Lodge, *Macromolecules*, 2007, **40**, 4048-4052.

61. P. Bhargava, Y. F. Tu, J. X. Zheng, H. M. Xiong, R. P. Quirk and S. Z. D. Cheng, *J. Am. Chem. Soc.*, 2007, **129**, 1113-1121.

62. L. Wang, X. F. Yu, S. G. Yang, J. X. Zheng, R. M. Van Horn, W. B. Zhang, J. T. Xu and S. Z. D. Cheng, *Macromolecules*, 2012, **45**, 3634-3638.

63. I. LaRue, M. Adam, M. Pitsikalis, N. Hadjichristidis, M. Rubinstein and S. S. Sheiko, *Macromolecules*, 2006, **39**, 309-314.

64. K. Schillén, W. Brown and R. M. Johnsen, *Macromolecules*, 1994, **27**, 4825-4832.

65. G. Landazuri, V. V. A. Fernandez, J. F. A. Soltero and Y. Rharbi, *J. Phys. Chem. B*, 2012, **116**, 11720-11727.

66. S. Y. Kim, K. E. Lee, S. S. Han and B. Jeong, *J. Phys. Chem. B*, 2008, **112**, 7420-7423.

67. Y. Y. Yuan and J. Wang, *Colloid Surf. B-Biointerfaces*, 2011, **85**, 81-85.

68. X. D. Ye, J. Y. Fei, K. Xu and R. K. Bai, *J. Polym. Sci. Part B: Polym. Phys.*,

2010, **48**, 1168-1174.

69. Y. S. Yu and A. Eisenberg, *J. Am. Chem. Soc.*, 1997, **119**, 8383-8384.

70. Y. S. Yu, L. F. Zhang and A. Eisenberg, *Macromolecules*, 1998, **31**, 1144-1154.

71. H. B. Du, J. T. Zhu and W. Jiang, *J. Phys. Chem. B*, 2007, **111**, 1938-1945.

72. N. Fairley, B. Hoang and C. Allen, *Biomacromolecules*, 2008, **9**, 2283-2291.

Graphic For Table of Content

Effect of local chain deformability on the temperature-induced morphological transitions of polystyrene-*b*-poly(*N*-isopropylacrylamide) micelles in aqueous solution

Xi-Xian Ke[1], Lian Wang[2], Jun-Ting Xu[1],* Bin-Yang Du[1], Ying-Feng Tu[3], Zhi-Qiang Fan[1]

[1]MOE Key Laboratory of Macromolecular Synthesis and Functionalization, Department of Polymer Science & Engineering, Zhejiang University, Hangzhou 310027, China
[2]College of Material, Chemistry and Chemical Engineering, Hangzhou Normal University, Hangzhou 310036, China
[3]Department of Polymer Science and Engineering, College of Chemistry, Chemical Engineering and Materials Science, Soochow University, Suzhou, 215123, P. R. China.

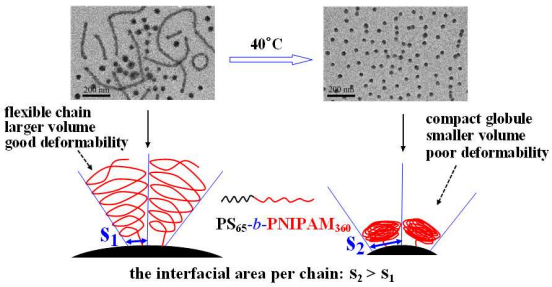

Local chain deformability is introduced to interpret abnormal temperature-induced morphological transitions of block copolymer micelles.